Hindawi
Discrete Dynamics in Nature and Society
Volume 2020, Article ID 6518531, 11 pages
https://doi.org/10.1155/2020/6518531

Research Article

Reaction Control System Optimization for Maneuverable Reentry Vehicles Based on Particle Swarm Optimization

Hang Gui, Ruisheng Sun, Wei Chen, and Bin Zhu

Nanjing University of Science and Technology, Nanjing 210094, China

Correspondence should be addressed to Ruisheng Sun; srscom@163.com

Received 3 October 2019; Revised 2 February 2020; Accepted 12 February 2020; Published 12 March 2020

Academic Editor: Giancarlo Consolo

This paper presents a new parametric optimization design to solve a class of reaction control system (RCS) problem with discrete switching state, flexible working time, and finite-energy control for maneuverable reentry vehicles. Based on basic particle swarm optimization (PSO) method, an exponentially decreasing inertia weight function is introduced to improve convergence performance of the PSO algorithm. Considering the PSO algorithm spends long calculation time, a suboptimal control and guidance scheme is developed for online practical design. By tuning the control parameters, we try to acquire efficacy as close as possible to that of the PSO-based solution which provides a reference. Finally, comparative simulations are conducted to verify the proposed optimization approach. The results indicate that the proposed optimization and control algorithm has good performance for such RCS of maneuverable reentry vehicles.

1. Introduction

Nowadays, hypersonic maneuverable reentry vehicles have received considerable attention from various countries, owing to its promising application in civilian and military aspects [1]. In the military, high mobility and large-scale hypersonic vehicles are characterized by their ability to cope with future near-space operations, break through ballistic defence systems, and achieve rapid global precision strikes. Usually, the initial reentry flight is with high altitude and thin atmosphere density, which results in low aerodynamic control efficiency. Reaction control system (RCS) is a kind of spacecraft system that uses thrusters arranged around the side direction of aircraft to provide attitude control torque [2], and sometimes translation force. Consequently, RCS is a better solution scheme to provide efficient control performance. Currently, a lot of research studies on RCS are focused on RCS thruster configuration [2], RCS nozzle selection logic [3, 4], and RCS combined with pneumatic rudder surface control [5, 6]. Liu provides a new method to obtain necessary and sufficient conditions for impulse controllability in continuous linear dynamics, which performs discrete-time actions for spacecraft maneuvering [7]. However, due to the discontinuity and limited working time of RCS, it is different from conventional continuous servo control.

At present, mathematical optimal control is divided into two categories, the direct method [8, 9] and indirect method [10, 11]. The direct method uses the original discrete optimal control problem as the parameter optimization problem and then finds the optimal solution through nonlinear programming [12, 13]. Generally, the direct method is more popular than the indirect method because the direct analytical solution of the complex nonlinear system is easier to solve [14, 15]. HP adaptive pseudospectral method is a combination of Legendre pseudospectral method and HP adaptive method. The HP adaptive pseudospectral method discretizes state variables and control variables into a series of Legendre–Gauss–Lombarto (LGL) points, which is one of the most popular and effective direct methods at present [16, 17]. Due to the nondifferentiability of RCS variables and flexible time interval, the application of pseudospectral method in RCS is limited, and the Karush–Kuhn–Tucker (KKT) condition is not satisfied.

In order to effectively solve such problems, some intelligent algorithms such as PSO algorithm, genetic

algorithm (GA), and neural network algorithm are becoming more and more attractive due to their high speed and high precision. These intelligent algorithms are inspired by natural phenomena, such as the association between ants, birds, and even human social behaviour [18, 19]. PSO was proposed by Eberhart and Kennedy [20] in 1995 and later promoted by other researchers [21]. Due to its advantages of simple theory, easy programming, and high computational efficiency, PSO has achieved excellent results in solving discontinuous problems. For example, Pires et al. proposed a new method to control the convergence rate of PSO algorithm in 2010 by using the concept of fractional calculus [22]. Unlike traditional optimization methods, PSO algorithm does not depend on the strict mathematical characteristics (derivability, continuity) and constraints of the optimization problem. In 2010, Yang et al. proposed a new method for solving missile fuel impulse optimal control problem using improved PSO technology, but this method did not consider the optimal operating mode and elastic interval [23]. Rahimi et al. proposed a novel PSO method to solve the optimal control problem of spacecraft reentry orbit, which avoided the computational burden of common analytical methods [24]. Zhou et al. using the particle swarm algorithm for the design of hypersonic vehicle guidance [25].

Therefore, a new method of solving RCS problem of maneuverable reentry vehicles with discrete and flexible time intervals by using improved particle swarm optimization (PSO) method is proposed in this paper. This discrete and flexible time optimization problem cannot be solved by HP adaptive pseudospectral method. The rest of this paper is organized as follows. In Section 2, the mathematical model of RCS control for maneuverable reentry vehicle is deduced, and the optimal RCS problem is given. Section 3 details the modifications based on basic PSO and RCS design. Aiming at the optimal setting of RCS control for maneuverable reentry vehicles, the structure and parameter design of the controller are discussed. On this basis, a suboptimal control guidance law based on PSO is proposed, which can be used in real-time designs. In Section 4, comparative simulations are conducted to verify the proposed optimization approach. The results indicate that the proposed optimization and control algorithm has good performance for such RCS of maneuverable reentry vehicles. Finally, Section 5 gives some conclusions of this paper.

2. Problem Description

2.1. Dynamics of the Vehicle System. The mathematical model of the maneuverable reentry vehicle includes the body dynamic model, the RCS thrust model, and the aerodynamic model, as well as the path constraint conditions during the reentry process of the vehicle [26, 27]. In order to facilitate discussion, only the motion of maneuverable reentry vehicle in longitudinal plane is considered, and the earth is assumed to be flat and stationary. Thus the dynamic equations are

$$\begin{cases} \dfrac{dV}{dt} = \dfrac{(P\cos\alpha - D - mg\sin\theta + u_{RCS}\cdot F_{RCS}\sin\alpha)}{m}, \\ \dfrac{d\theta}{dt} = \dfrac{(P\sin\alpha + L - mg\cos\theta - u_{RCS}\cdot F_{RCS}\cos\alpha)}{(mV)}, \\ \dfrac{dx}{dt} = V\cos\theta, \\ \dfrac{dy}{dt} = V\sin\theta, \\ \dfrac{d\omega_z}{dt} = \dfrac{\left(u_{RCS}\cdot F_{RCS}\cdot X_{cg} + M_z\right)}{J_z}, \\ \dfrac{d\vartheta}{dt} = \omega_z, \\ \dfrac{dm}{dt} = -m_c, \\ \dfrac{dI_{RCS}}{dt} = \left|u_{RCS}\right|\cdot F_{RCS}, \\ \alpha = \vartheta - \theta, \end{cases} \tag{1}$$

where the state variables include flight velocity V, the horizontal position x, trajectory inclination angle θ, height position y, pitch angular ratio ω_z, pitch angle ϑ, gravity acceleration g, mass of the reentry vehicle m, and RCS thrust total impulse I_{RCS}. Engine thrust P, RCS thrust F_{RCS}, RCS thrust to centroid distance X_{cg}. u_{RCS} is the switching quantity of the RCS nozzle, which has three states: 1, 0, −1. J_z is the moment of inertia of the z-axis. m_c is mass flow. α means the attack of angle (Figure 1). The lift force L, drag force D, and aerodynamic pitch moment M_z are all the functions of reference area S, dynamic pressure q, and reference length l. The lift, drag, and pitch moment coefficients C_L, C_D, and m_z are shown in equation (2).

$$\begin{cases} Ma = \dfrac{V}{\text{Sonic}}, \\ L = qSC_L(\alpha, Ma), \\ D = qSC_D(\alpha, Ma), \\ M_z = qSlm_z(\alpha, Ma). \end{cases} \tag{2}$$

The Mach number Ma here is a function of velocity V and local sonic speed.

The RCS can rapidly provide thrust force and control torque to maneuverable reentry vehicle by a nozzle switch. Since the nozzle switch between ON and OFF is very fast, the switching time delay here can be almost ignored. Thus, the RCS thrust model is

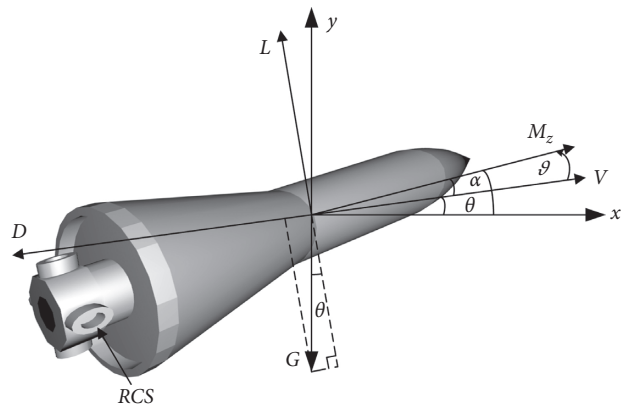

Figure 1: Motion coordinate systems of the maneuverable reentry vehicle. This is the basic shape of the maneuverable reentry, with the tail of the main engine and the RCS nozzle.

$$F_i = \begin{cases} F_{RCS}, & U = 1, \\ 0, & U = 0, \end{cases} \tag{3}$$

where F_i is the thrust force generated by the nozzle i. U is switch instruction of the nozzle, 0 means OFF, 1 means ON. RCS nozzles are generally symmetrically arranged, and the resulting control torque is shown in Figure 2.

2.2. Constraints during Flight Process

2.2.1. Path Constraints. During the reentry phase, to ensure the structural safety of the maneuverable reentry vehicle, the constraints of dynamic pressure and angle of attack must be strictly satisfied, and the reentry trajectory should be as smooth as possible [28].

(a) Dynamic pressure: dynamic pressure is an important characteristic variable in aerodynamics. The dynamic pressure at the reentry stage strictly meets the following constraints:

$$q = \frac{\rho V^2}{2} < q_{\max}. \tag{4}$$

(b) Angle of attack: the angle of attack is an important state variable in flight dynamics, which determines the heat rate and overload experienced by the reentry vehicle. The angle of attack during the reentry phase strictly meets the following constraints:

$$\alpha_{\min} < \alpha < \alpha_{\max}. \tag{5}$$

2.2.2. Terminal Constraint. In order to ensure the terminal guidance, the terminal guidance status during the reentry phase must satisfy the terminal constraints [28]. The error of the trajectory inclination angle θ inclination should be less than a certain value, i.e.

$$\theta_{\min} < \theta < \theta_{\max}. \tag{6}$$

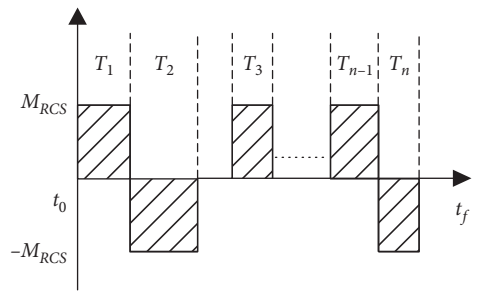

Figure 2: Schematic of RCS control torque. The horizontal axis is the working time, and the vertical axis is the control torque generated by the RCS.

2.2.3. Control Constraints. Due to the fuel limitation and nozzle switch delay of RCS, we consider total working time and minimum working time limitation [29], i.e.

$$\begin{cases} \sum_{i=1}^{n} T_i \le T_{\text{Total\_Max}}, \\ T_i \ge T_{\text{Min}}. \end{cases} \tag{7}$$

2.3. Objective of the System Design.

For maneuverable reentry vehicles, the accuracy of control and the fuel consumption of RCS are a contradictory relationship. If high control accuracy is required, the nozzle must be opened frequently to consume fuel. Considering that the RCS fuel of the maneuverable reentry vehicle is limited, the purpose of optimizing the RCS thrust control is to ensure the control accuracy while reducing the amount of fuel consumed. Therefore, the objective function J for minimizing control energy and control errors is written as

$$\min J = \lambda \frac{\int_{t_0}^{t_f} |u| F_{RCS} \mathrm{d}t}{I_{RCS}} + \int_{t_0}^{t_f} e(t)^2 \mathrm{d}t, \tag{8}$$

where λ is the weight coefficient, u means the switching quantity of the RCS nozzle, and the control error $e(t) = x_1 - x_c = \theta - \theta_c$. Here t_0 and t_f, respectively, represent the initial and end times.

Obviously, the above design is optimization problem with various constraints, so how to transform a constrained optimization problem to an unconstrained optimization problem will make the design easier. Penalty function method is a good way to do this [26]. In order to enhance the computational efficiency of trajectory optimization, penalty function $P(t)$ can be introduced to rewrite the objective function [30, 31]. When the constraints in Section 2.2 are not satisfied, $P(t)$ will take a very large value to penalize the objective function. So equation (8) can be modified as follows:

$$\min J = \lambda \frac{\int_{t_0}^{t_f} |u| F_{RCS} \mathrm{d}t}{I_{RCS}} + \int_{t_0}^{t_f} e(t)^2 \mathrm{d}t + \mu P(t), \tag{9}$$

where μ is the penalty factor which is positive.

3. Optimization and Control Design

3.1. Optimal Design Based on Improved PSO. PSO algorithm is one of popular optimization techniques, which was originally developed to graphically simulate the bird flock. The birds form groups and move in a flock, and each bird is a particle. Each particle is assumed to have two characteristics: position and velocity. Each particle wanders around in the design space and remembers the best position (in terms of objective function value) it has discovered. The particles communicate information or good positions to each other and adjust their individual positions and velocities based on the information received on the good positions [32]. Several variants of the PSO technique have been proposed so far, following Eberhart and Kennedy [33, 34].

Here we define the notation: assuming the search space is d-dimensional, the i-th particle of the group is represented by a d-dimensional vector $x_i = \{x_{i1}, x_{i2}, \ldots, x_{id}\}$, and the experienced best position is expressed as $p_i = \{p_{i1}, p_{i2}, \ldots, p_{id}\}$. The particle the best position that has been experienced is $g_i = \{g_n, g_{i2}, \ldots, g_{id}\}$ and the position change (velocity) of the i-th particle is $v_i = \{v_{i1}, v_{i2}, \ldots, v_{i3}\}$ [21]. During the iteration, particle i updates its position and velocity according to the following formulas:

$$v_{id}^{k+1} = w \cdot v_{id}^{k} + c_1 \cdot \text{rand} \cdot \left(p_{id}^{k} - x_{id}^{k}\right) + c_2 \cdot \text{rand} \cdot \left(g_{id}^{k} - x_{id}^{k}\right), \tag{10}$$

$$x_{id}^{k+1} = x_{id}^{k} + v_{id}^{k+1}, \tag{11}$$

where w is the inertia weight, c_1, c_2 are the acceleration factors, k is the iteration counter, and rand() is a random number between (0, 1). In addition, the velocity of each dimension of the particle is limited by the maximum velocity $v_{\max}$. When the value of $v_{\max}$ is large, the particle can fly fast, which is conducive to global search, but it is possible to fly over the optimal solution. When $v_{\max}$ is small, the particle can be searched in the feature area, but it is easy to fall into the local optimal solution.

The inertia weight w was originally introduced by Eberhart and Shi [35]. When using PSO found that usually the particle velocities build up too fast and the minimum of the objective function is easily skipped [32]. Hence, an inertia weight w is added to reduce the velocity. Generally, the value of w is assumed to be a constant. A large value of w promotes global exploration and a smaller value promoted a local search. Therefore, to achieve a balance between global and local exploration to speed up convergence to the true optimum, we design the inertia weight as an exponentially decreasing function. The exponentially changing inertia weight coefficient w can achieve better global optimization capabilities in the initial stage of optimization and better local optimization capabilities in the later stages of optimization, i.e.,

$$w = (w_0 - w_\infty)e^{-k} + w_\infty. \tag{12}$$

Simultaneously, RCS is a class of discontinuous actuators with limitation of fuel consumption. Consequently, we select the switch state u_i and working time T_i as design variables, where u_i is discrete, and T_i is continuous. Since the movement of the particle position is a continuous process, the particle position vector is corresponded to the design variable by a sign function.

Therefore, we define the structure of the particle's position vector x_i and sign function sign(x). $\{u_1, u_2, \ldots, u_{id/2}\}$ and $\{T_1, T_2, \ldots, T_{id/2}\}$ form a complete RCS nozzle assignment.

$$\text{sign}(x) = \begin{cases} +1\,(x > 0.5), \\ 0\,(-0.5 < x < 0.5), \\ -1\,(x < -0.5), \end{cases}$$

$$\begin{bmatrix} u_{i1} \\ T_{i1} \\ u_{i2} \\ T_{i2} \\ \vdots \\ u_{id/2} \\ T_{id/2} \end{bmatrix} = \begin{bmatrix} \text{sign}\left(x_{i1}\right) \\ x_{i2} \\ \text{sign}\left(x_{i3}\right) \\ x_{i4} \\ \vdots \\ \text{sign}\left(x_{i(d-1)}\right) \\ x_{id} \end{bmatrix} = x_i. \tag{13}$$

The upper and lower bounds of the RCS nozzle switch state u_i and working time T_i are defined as

$$\begin{cases} u_{\max} = +1, \\ u_{\min} = -1, \\ T_{\max} = 5s, \\ T_{\min} = 0.1s. \end{cases} \tag{14}$$

3.2. Improved PSO Algorithm Process. Combined with the algorithm described in Section 3.1, the entire calculation process is depicted in Figure 3. The specific steps are as follows:

(1) The initial trajectory parameters include the initial velocity, position, and attitude of the maneuvering reentry vehicle. PSO initialization includes setting group size, neighborhood size, iteration times, acceleration coefficient, inertia weight, random group position, and speed.

(2) The inertia weight coefficient w and the particle velocity v_{id}^{k+1} and position x_{id}^{k+1} information are updated according to equations (10)–(12).

(3) Get u_i and T_i as control variables based on the updated particle position.

(4) Input control variables u_i and T_i into trajectory program for calculation. Since the RCS nozzle switch status is only (1, 0, −1), so $u_i = \text{sign}(u_i)$.

(5) The value of objective function J was calculated to update the individual optimal fitness and population optimal fitness.

(6) Determine whether the new particles generated by iteration reach the minimum objective value or

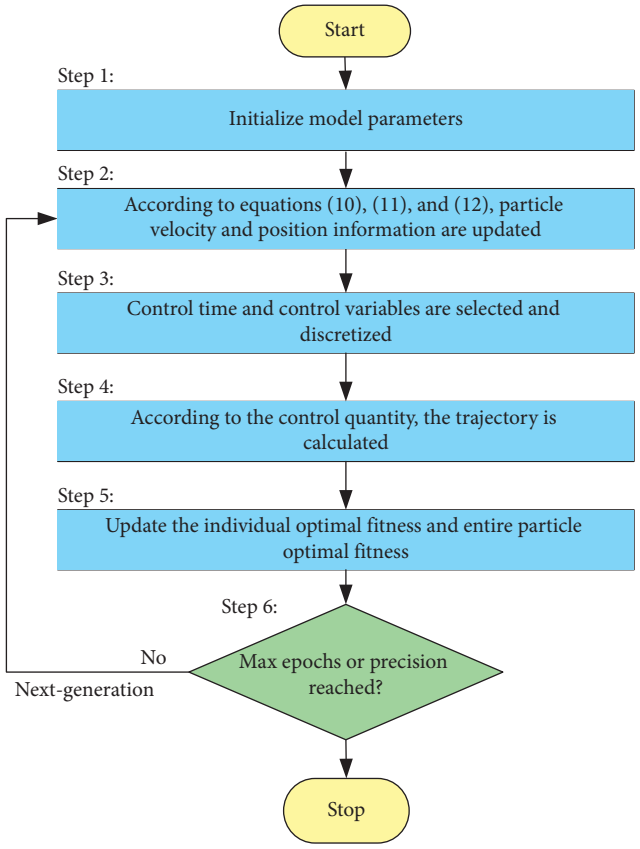

FIGURE 3: Process of propose PSO algorithm. After the optimization program starts, the particle is initialized first and then iteratively calculated according to the algorithm until the program is terminated after the stop condition is satisfied.

whether the number of iterations reaches the preset maximum value. If one of these two conditions is satisfied, the optimal solution of the problem corresponds to the global optimal solution of the particle and stops iteration. Otherwise, go to step (2) to update the position and velocity of particles in the next iteration.

3.3. Suboptimal Online Controller Design. Through the particle swarm optimization method, the optimal solution of the maneuverable reentry vehicle is obtained, which minimizes the RCS consumption and control error. Obviously, the particle swarm algorithm spent long time to converge, which cannot satisfy real-time control requirements [14]. Therefore, it is very important to find an online control scheme to obtain a suboptimal control design. By tuning the suboptimal control parameters, we here try to acquire efficacy as close as possible to that of the PSO-based solution. Figure 4 shows the guidance and control process of maneuverable reentry vehicle.

For the optimal flight control problem consideration of equation (1) and Figure 4, the mathematical model based on disturbance linearization motion can be used as a reference model for the controlled object [14].

$$\dot{\mathbf{x}} = \mathbf{A}\mathbf{x} + \mathbf{B}\mathbf{u}, \tag{15}$$

where $\mathbf{x} = \begin{bmatrix} x_1 \\ x_2 \\ x_3 \end{bmatrix} = \begin{bmatrix} \theta \\ \dot{\theta} \\ \ddot{\theta} \end{bmatrix}$, $\mathbf{A} = \begin{bmatrix} 0 & 1 & 0 \\ 0 & 0 & 1 \\ 0 & -1/T_M^2 & -2\xi_M/T_M \end{bmatrix}$, $\mathbf{B} = \begin{bmatrix} 0 \\ 0 \\ K_M \end{bmatrix}$. Here K_M, ξ_M, and T_M, respectively, represent the transfer coefficient, damping, and time constant of the vehicle.

It can be seen from the schematic diagram of the guidance control system of the maneuverable reentry vehicle shown in Figure 4. The detailed control structure is shown in Figure 5, where $f(e(t))$ is the RCS designed with reference model. The work of this paper is mainly divided into two steps: (1) In the previous section, the PSO numerical optimization method was used to obtain the optimal RCS numerical solution; (2) in this section, the suboptimal online controller will be determined by establishing the mathematical relationship between the error $e(t)$ and the control u_{RCS}.

Pulse width pulse frequency (PWPF) modulator is a popular technique used in RCS nozzle control [36, 37], which is designed by combining a first-order filter and a Schmitt trigger in the feedforward loop (Figure 5) [5, 38]. PWPF modulator is widely used in spacecraft control systems [6] because it works with an almost linear input/output relationship which makes the design easier. The first-order filter has the transfer function $f(s)$:

$$f(s) = \frac{K}{Ts + 1}. \tag{16}$$

The Schmitt trigger [5, 39] is a switching relay with hysteresis and dead zone, as shown in Figure 5. The mathematical description of the Schmitt trigger is formulated as [37, 39]

$$u = \begin{cases} +1, & e \geq U_{\text{on}}, \\ +1, & U_{\text{off}} \leq e < U_{\text{on}}, \dot{e} < 0, \\ 0, & -U_{\text{on}} \leq e < U_{\text{off}}, \dot{e} < 0, \\ 0, & -U_{\text{off}} \leq e < U_{\text{on}}, \dot{e} > 0, \\ -1, & -U_{\text{on}} \leq e - U_{\text{off}}, \dot{e} > 0, \\ -1, & e < -U_{\text{on}}. \end{cases} \tag{17}$$

Subject to the following restrictions:

(1) Due to the fuel limitations carried by the RCS system, the total working time of the nozzle is shown in equation (7)

(2) According to the discrete characteristics of the RCS nozzle, the generated control torque is as follows:

$$M_c = \begin{cases} M_{RCS}, & (u = 1), \\ 0, & (u = 0), \\ -M_{RCS}, & (u = -1), \end{cases} \tag{18}$$

where M_c is the control torque generated by the RCS nozzle.

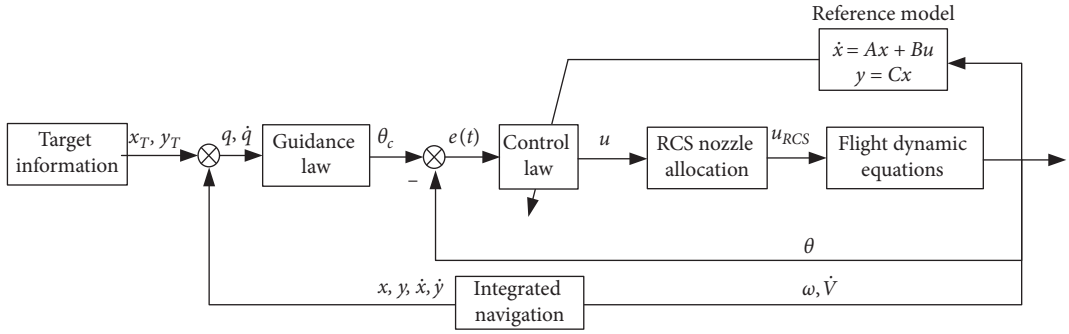

Figure 4: Guidance and control structure of maneuverable reentry vehicle. A guidance command is generated according to the guidance law by the current location information and the location information of the target. The control system controls the nozzle according to the guidance command.

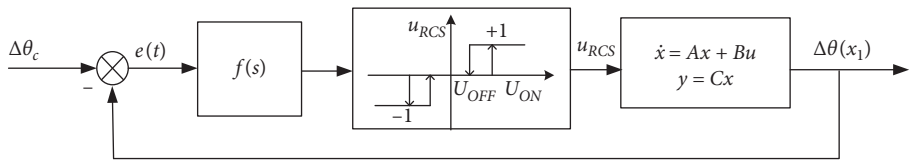

Figure 5: Structure of RCS.

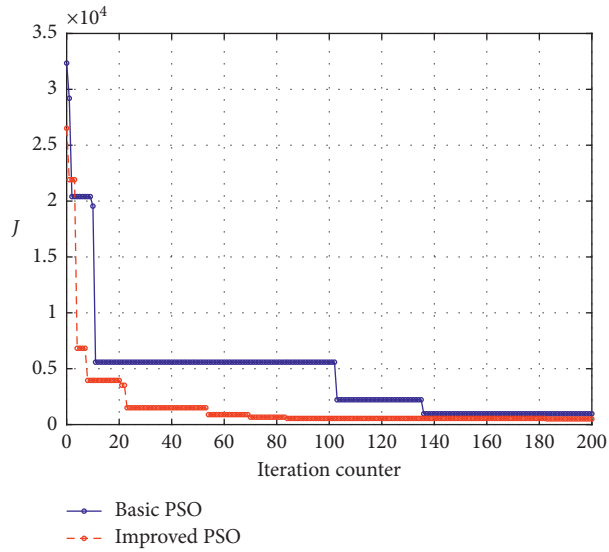

Figure 6: Curve of objective function J with iteration counter.

By selecting suitable parameters K, T, U_{on}, and U_{off}, the online control effect is as close as possible to the trajectory optimization result of PSO [14]. Similarly, the online controller parameters can also be optimized by using the PSO method.

3.4. Guidance Law Design. Guidance can be defined as a method of guiding and controlling the flight of a vehicle toward a target. We need to design an appropriate guidance law to enable the maneuvering reentry vehicle along the predetermined trajectory, that is, to express guidance law in terms of the relative relationship between the vehicle and the target. Proportional navigation (PN) is one of the most popular guidance methods [40, 41]. Here, considering the influence of gravity, a modified PN law is expressed as

$$\dot{\theta}_c = K_1 \dot{q} + K_2 \frac{g}{V} \cos\theta, \tag{19}$$

where $\dot{\theta}_c$ is guidance command, and K_1, K_2 are guidance gains.

According to equation (19), the guidance law can be written in an integral formation:

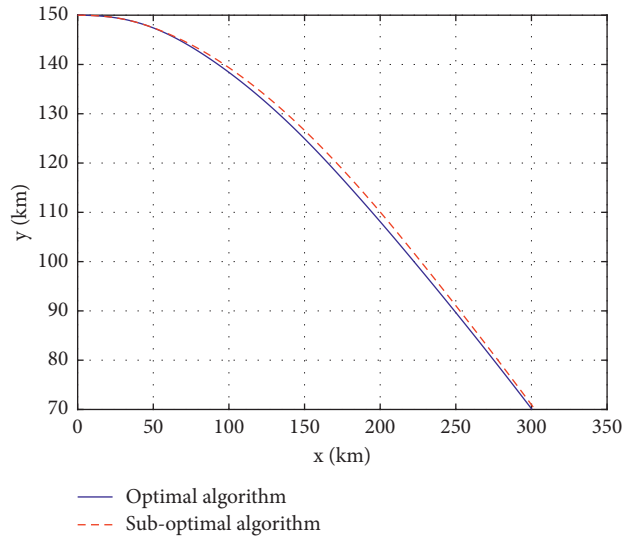

Figure 7: Trajectory curves under different conditions.

$$\theta_c(t) - \theta_0(t_0) = K_1(q(t) - q(t_0)) + K_2 \int_{t_o}^{t} \left(\frac{g}{V}\cos\theta\right) dt. \tag{20}$$

4. Numerical Simulations

In this section, trajectory simulations are presented to verify the efficacy of nonlinear RCS suboptimal control algorithm in detail. The fourth-order Runge–Kutta method is used to integrate the dynamic model. The simulation parameters are as follows: the *RCS* control force $F_{RCS} = 150$ N, minimum switching time of nozzle $T_{\min} = 0.1$ s, and maximum working time $T_{\text{total\_Max}} = 80$ s. Initial state values of the maneuverable reentry vehicle: $t_0 = 0$ s, $m_0 = 1248.95$ kg, $v_0 = 2500$ m/s, $x_0 = 0$ m, $y_0 = 150000$ m, $\omega_{z0} = 0$ rad/s, $= 0$ deg, $\vartheta_0 = \theta_0 = 0$ deg, $l = 2.14$ m. Main engine thrust $P = 40$ kN, mass flow $m_c = 10$ kg/s, working time 60 s. Target position $x = 300$ km and the end condition of the trajectory calculation is that the height reaches 70 km reentry height.

4.1. Efficacy of Improved PSO Algorithm. Here in order to validate the performance of the improved PSO, comparative simulations are conducted between improved PSO with exponential decreasing inertia weight and basic PSO with constant inertia weight. The initial conditions for the optimization design are set as follows. The control parameters of PSO are particle number $m = 10$, dimension $n = 100$, $c_1 = c_2 = 1.8$. The constant inertia weight $w = 0.8$, exponential decreasing inertial weight $w = (1 - 0.8)e^{-0.03k} + 0.8$, and the number of iteration reaches 200. The objective function J results are shown in Figure 6.

As shown in Figure 6, the value of objective function with improved PSO method drops faster than that with basic PSO in the initial stage, which indicates its better global optimization ability. At the later stage of optimization, the value of objective function with improved PSO is smaller, which indicates that it has better local optimization capabilities. It is seen that the objective function value remains at the same value for a long iteration period, which indicates that the particles have reached the global optimum point in the feasible area.

4.2. Verification of Suboptimal Algorithm. Controller gains are $K = 1$, $T = 0.05$. The parameters of the Schmitt trigger $U_{\text{on}} = 1$, $U_{\text{off}} = 0.1$. Additionally, α is chosen as a state constraint of $\alpha_{\text{lower}} = -15$ deg, $\alpha_{\text{upper}} = +15$ deg. Comparative simulation results between optimal and suboptimal algorithms are shown in Figures 7–13.

From Figures 7–13, it can be concluded that

(1) Figures 7 and 8 show that the trajectory and velocity curves with the optimal PSO algorithm are similar to those with the suboptimal online algorithm, which indicates that the online design has good performance.

(2) Figures 9–11 indicate that the velocity inclination θ of the optimal trajectory is smoother than that of the suboptimal trajectory. From the angle of attack and pitch curve (Figures 10 and 11), it can be seen that the oscillation amplitude of the optimal trajectory is smaller. In addition, there is a high maneuverable with large angle of attack at the initial stage of optimal scheme, and then the angle of attack gradually converges to zero. Because the direction of the velocity is easier to change at lower speed, maneuverable at this time is beneficial to the overall trajectory performance. Also we find that the changing trend of angle of attack with suboptimal online control is similar to that of PSO scheme.

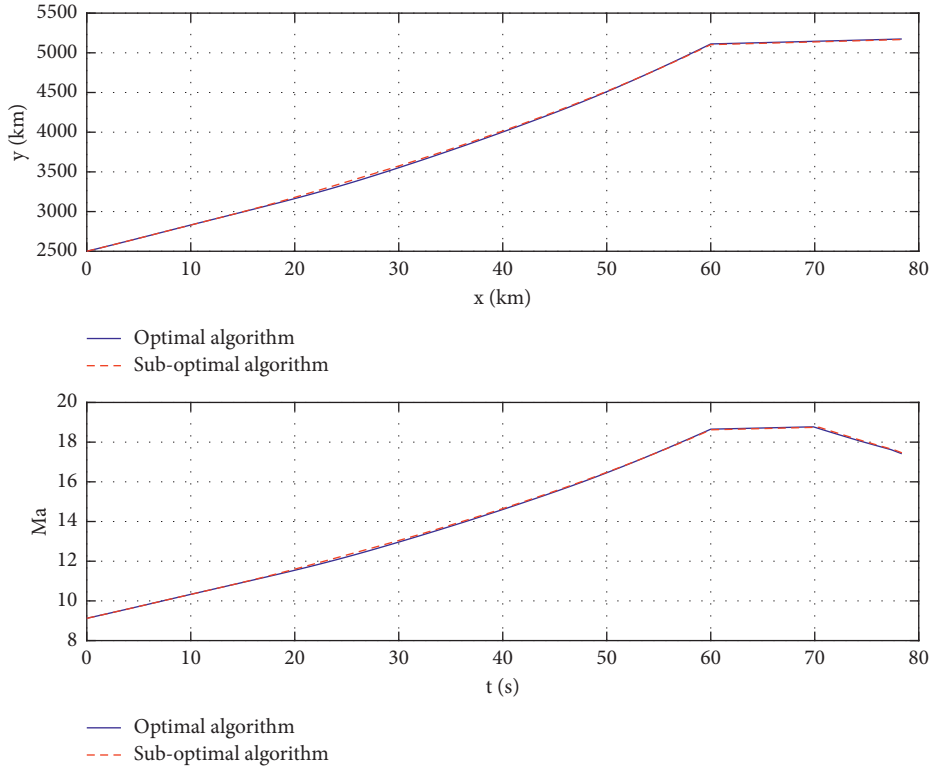

Figure 8: Curve of Ma, V and t.

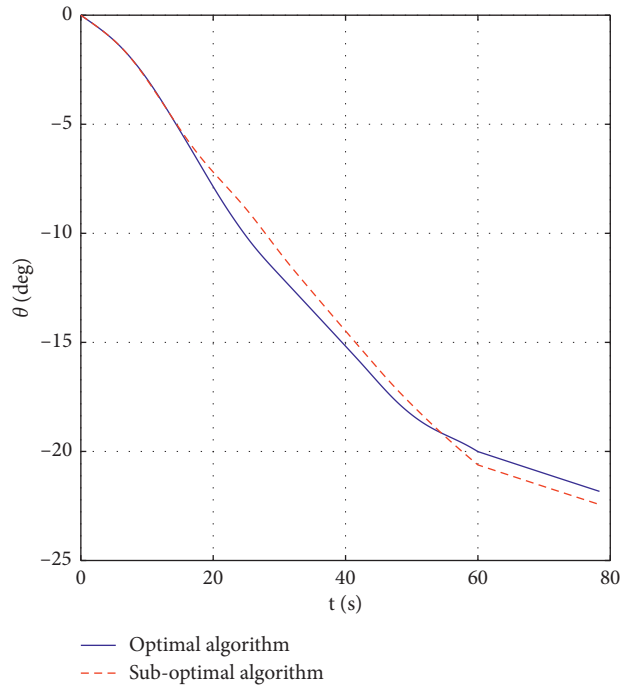

Figure 9: Curve of θ and t.

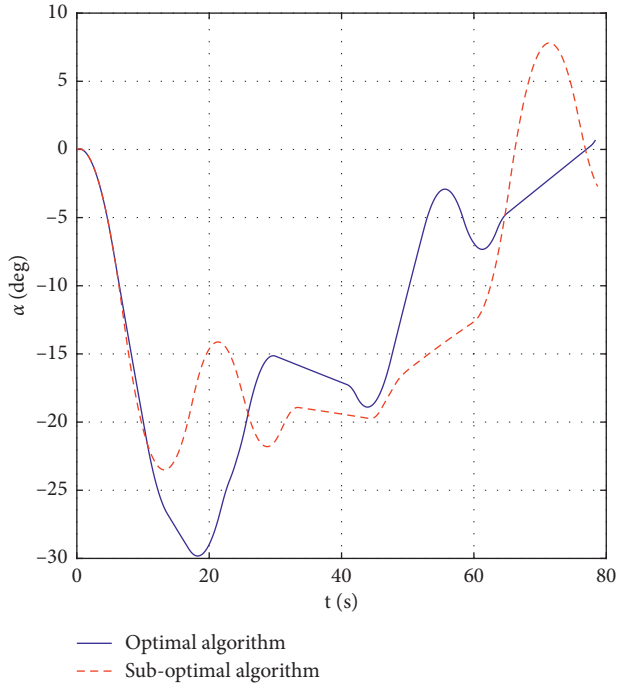

Figure 10: Curve of α and t.

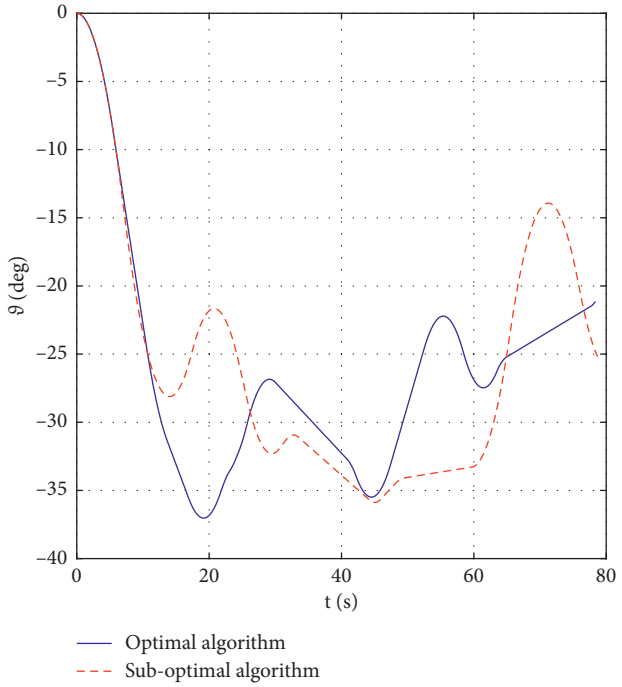

Figure 11: Curve of ϑ and t.

(3) As shown in Figures 12 and 13, it can be indicated that the RCS nozzle with suboptimal scheme has very close opening time and total impulse consumption to that of the PSO algorithm, which verifies the effectiveness of the propose algorithm.

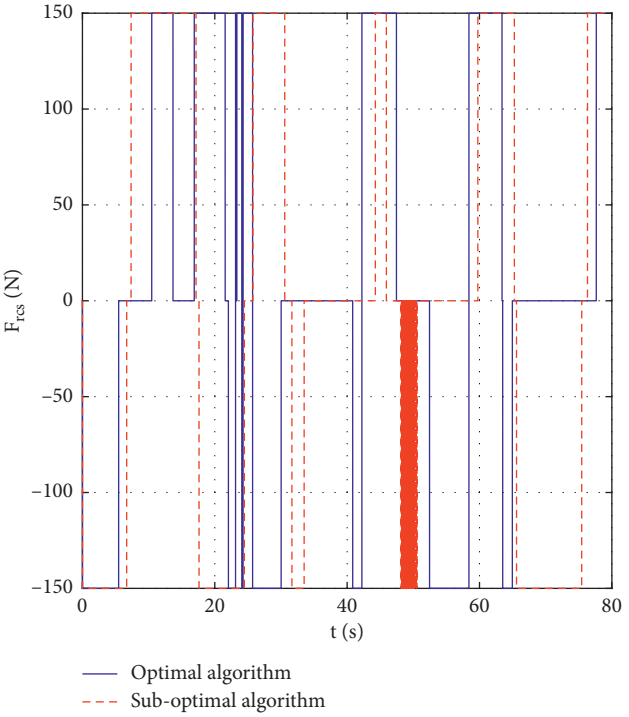

Figure 12: Curve of F_{RCS} and t.

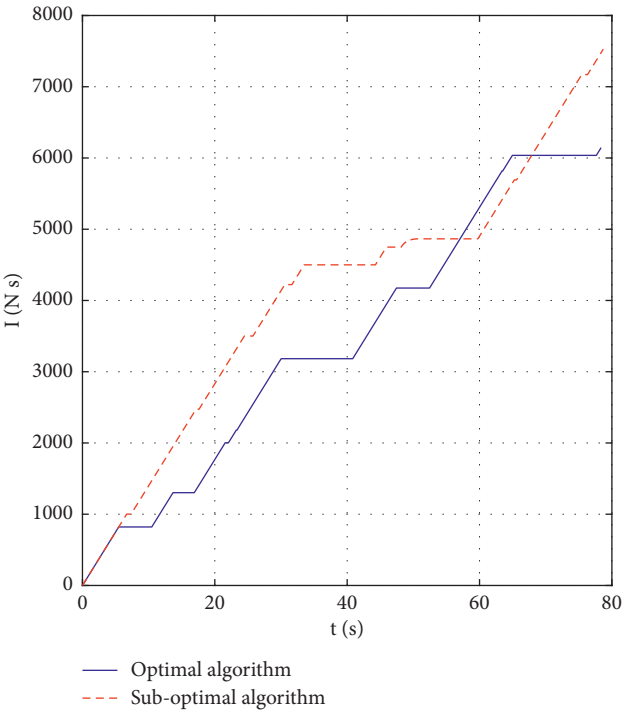

Figure 13: Curve of I_{RCS} and t.

5. Conclusions

Based on the basic particle swarm optimization (PSO) method, an exponentially decreasing inertia weight

function is introduced to improve convergence performance of the PSO algorithm. Considering PSO algorithm spends long calculation time, a suboptimal control and guidance scheme is developed for online practical design. By tuning the control parameters, we try to acquire efficacy as close as possible to that of the PSO-based solution which provides a reference. Finally, comparative simulations are conducted to verify the proposed optimization approach. The results indicate that the proposed optimization and control algorithm has good performance for such RCS of maneuverable reentry vehicles. This paper proposes a new parametric optimization design to solve a class of reaction control system (RCS) problem with discrete switching state, flexible working time, and finite-energy control for maneuverable reentry vehicles. In order to enhance the nonlinear global optimization capacity, an improved PSO algorithm is used to find the optimal setting of the RCS nozzle control variable by selecting the switch state and working time as the RCS nozzle. For practical application requirements, a suboptimal guidance scheme is online designed. The simulation results demonstrate that the online control algorithm has good performance, which is very close to the optimal scheme. The closed-loop system has good performance, satisfy the process constraints and limitation of fuel consumption.

Meanwhile, the proposed PSO control method can be extended to the composite control with RCS and pneumatic control for reentry vehicles. The real-time online programming of the PSO algorithm has attracted more and more attention, but the further improvement of the convergence speed of the PSO has yet to be resolved.

Data Availability

The data used to support the findings of this study are available from the corresponding author upon request.

Conflicts of Interest

The authors declare that there are no conflicts of interest regarding the publication of this article.

Acknowledgments

This work was supported by the Natural Science Foundation of China (NSFC) under Grant No. 11176012 and 51809138.

References

[1] X. Shao and H. Wang, "Active disturbance rejection based trajectory linearization control for hypersonic reentry vehicle with bounded uncertainties," *ISA Transactions*, vol. 54, pp. 27–38, 2015.

[2] T. W. Hwang, C.-S. Park, M.-J. Tahk, and H. Bang, "Upper-stage launch vehicle servo controller design considering optimal thruster configuration," in *Proceedings of AIAA Guidance, Navigation, and Control Conference and Exhibit*, p. 5330, Austin, TX, USA, August 2003.

[3] K. A. Wise and D. J. B. roy, "Agile missile dynamics and control," *Journal of Guidance, Control, and Dynamics*, vol. 21, no. 3, pp. 441–449, 1998.

[4] J. He, R. Qi, B. Jiang, and R. Zhai, "Fault-tolerant control with mixed aerodynamic surfaces and RCS jets for hypersonic reentry vehicles," *Chinese Journal of Aeronautics*, vol. 30, no. 2, pp. 780–795, 2017.

[5] X. Wang, D. Wang, S. Zhu, and E. K. Poh, "Fractional describing function analysis of PWPF modulator," *Mathematical Problems in Engineering*, vol. 2013, Article ID 287040, 5 pages, 2013.

[6] T. C. Anthony, B. Wie, and S. Carroll, "Pulse-modulated control synthesis for a flexible spacecraft," *Journal of Guidance, Control, and Dynamics*, vol. 13, no. 6, pp. 1014–1022, 1990.

[7] X. Liu and A. R. Willms, "Impulsive controllability of linear dynamical systems with applications to maneuvers of spacecraft," *Mathematical Problems in Engineering*, vol. 2, no. 4, pp. 277–299, 1996.

[8] P. J. Enright and B. A. Conway, "Discrete approximations to optimal trajectories using direct transcription and nonlinear programming," *Journal of Guidance, Control, and Dynamics*, vol. 15, no. 4, pp. 994–1002, 1992.

[9] C. R. Hargraves and S. W. Paris, "Direct trajectory optimization using nonlinear programming and collocation," *Journal of Guidance, Control, and Dynamics*, vol. 10, no. 4, pp. 338–342, 1987.

[10] C. L. Ranieri and C. A. Ocampo, "Indirect optimization of three-dimensional finite-burning interplanetary transfers including spiral dynamics," *Journal of Guidance, Control, and Dynamics*, vol. 32, no. 2, pp. 445–455, 2009.

[11] J. A. Kechichian, "Optimal low-earth-orbit-geostationary-earth-orbit intermediate acceleration orbit transfer," *Journal of Guidance, Control, and Dynamics*, vol. 20, no. 4, pp. 803–811, 1997.

[12] F. Jiang, H. Baoyin, and J. Li, "Practical techniques for low-thrust trajectory optimization with homotopic approach," *Journal of Guidance, Control, and Dynamics*, vol. 35, no. 1, pp. 245–258, 2012.

[13] R.-s. Sun and C. Ming, "Velocity control for coning motion missile system using direct discretization method," *Discrete Dynamics in Nature and Society*, vol. 2015, Article ID 716547, 10 pages, 2015.

[14] R. Sun, Q. Hong, and G. Zhu, "A novel optimal control method for impulsive-correction projectile based on particle swarm optimization," *Discrete Dynamics in Nature and Society*, vol. 2016, Article ID 5098784, 9 pages, 2016.

[15] G. Zhao, Z.-g. Su, J. Zhan, H. Zhu, and M. Zhao, "Adaptively receding galerkin optimal control for a nonlinear boiler-turbine unit," *Complexity*, vol. 2018, Article ID 8643623, 13 pages, 2018.

[16] C. L. Darby, W. W. Hager, and A. V. Rao, "Direct trajectory optimization using a variable low-order adaptive pseudospectral method," *Journal of Spacecraft and Rockets*, vol. 48, no. 3, pp. 433–445, 2011.

[17] M. M. Khader, N. H. Sweilam, and W. Y. Kota, "Cardinal functions for Legendre pseudo-spectral method for solving the integro-differential equations," *Journal of the Egyptian Mathematical Society*, vol. 22, no. 3, pp. 511–516, 2014.

[18] K. Premalatha and A. Natarajan, "Hybrid PSO and GA for global maximization," *International Journal of Open Problems in Computer Science and Mathematics*, vol. 2, no. 4, pp. 597–608, 2009.

[19] M. A. El-Shorbagy and A. E. Hassanien, "Particle swarm optimization from theory to applications," *International Journal of Rough Sets and Data Analysis*, vol. 5, no. 2, pp. 1–24, 2018.

[20] R. Eberhart and J. Kennedy, "A new optimizer using particle swarm theory," in *Proceedings of the Sixth International Symposium on Micro Machine and Human Science. MHS'95*, IEEE, New York, NY, USA, pp. 39–43, October 1995.

[21] E. C. Laskari, K. E. Parsopoulos, and M. N. Vrahatis, "Particle swarm optimization for integer programming," in *Proceedings of the 2002 Congress on Evolutionary Computation. CEC'02 (Cat. No. 02TH8600)*, vol. 2, IEEE, Honolulu, HI, USA, pp. 1582–1587, May 2002.

[22] E. S. Pires, J. T. Machado, P. de Moura Oliveira, J. B. Cunha, and L. Mendes, "Particle swarm optimization with fractional-order velocity," *Nonlinear Dynamics*, vol. 61, no. 1-2, pp. 295–301, 2010.

[23] H. Yang, L. Dou, and M. Gan, "A particle swarm optimization for fuel-optimal impulsive control problems of guided projectile," in *Proceedings of Chinese Control and Decision Conference*, pp. 3034–3038, IEEE, Xuzhou, China, May 2010.

[24] A. Rahimi, K. Dev Kumar, and H. Alighanbari, "Particle swarm optimization applied to spacecraft reentry trajectory," *Journal of Guidance, Control, and Dynamics*, vol. 36, no. 1, pp. 307–310, 2012.

[25] H. Zhou, X. Wang, B. Bai, and N. Cui, "Reentry guidance with constrained impact for hypersonic weapon by novel particle swarm optimization," *Aerospace Science and Technology*, vol. 78, pp. 205–213, 2018.

[26] J. J. Pan, K. Feng, L. I. Huan-Liang, and X. Q. Yang, "Ballistic method of mine-laying rocket based on multi-objective particle swarm optimization," *Fire Control & Command Control*, vol. 43, no. 1, pp. 157–161, 2018, in Chinese.

[27] N. A. Shneydor, *Missile Guidance and Pursuit: Kinematics, Dynamics and Control*, Elsevier, Amsterdam, Netherlands, 1998.

[28] H. Duan and S. Li, "Artificial bee colony-based direct collocation for reentry trajectory optimization of hypersonic vehicle," *IEEE Transactions on Aerospace and Electronic Systems*, vol. 51, no. 1, pp. 615–626, 2015.

[29] B. Wie, *Space Vehicle Dynamics and Control*, American Institute of Aeronautics and Astronautics, Reston, VA, USA, 2008.

[30] J. Guo, S.-J. Tang, X. Li, and C.-L. Yang, "Optimum design of the project trajectory based on an improved particle swarm optimization," *Transactions of Beijing Institute of Technology*, vol. 30, no. 6, pp. 688–692, 2010, in Chinese.

[31] C. Jing, "Ballistic method based on improved particle swarm optimization algorithm," *Journal of Southeast University (Natural Science Edition)*, vol. 43, no. S1, pp. 215–218, 2013, in Chinese.

[32] S. S. Rao, *Engineering Optimization: Theory and Practice*, John Wiley & Sons, Hoboken, NJ, USA, 2019.

[33] R. Eberhart, P. Simpson, and R. Dobbins, *Computational Intelligence PC Tools*, Academic Press Professional, Inc., Cambridge, MA, USA, 1996.

[34] J. Kennedy and R. Eberhart, "Particle swarm optimization (PSO)," in *Proceedings of IEEE International Conference on Neural Networks*, pp. 1942–1948, Perth, Australia, December 1995.

[35] Y. Shi and R. C. Eberhart, "Parameter selection in particle swarm optimization," in *Proceedings of International Conference on Evolutionary Programming*, pp. 591–600, Springer, San Diego, CA, USA, July 1998.

[36] K. H. Kienitz and J. Bals, "Pulse modulation for attitude control with thrusters subject to switching restrictions," *Aerospace Science and Technology*, vol. 9, no. 7, pp. 635–640, 2005.

[37] E. Chegeni, M. Zandieh, and J. Ebrahimi, "Attitude control of satellite with PWPF modulator using predictive control algorithms," *Majlesi Journal of Electrical Engineering*, vol. 8, no. 3, pp. 25–31, 2014.

[38] W. Xinsheng and Z. Huaqiang, "Fractional order controller for satellite attitude control system with PWPF modulator," in *Proceedings of 34th Chinese Control Conference*, pp. 5758–5763, IEEE, Hangzhou, China, Hangzhou, China, July 2015.

[39] Y. Lian and G. Tang, "Libration point orbit rendezvous using PWPF modulated terminal sliding mode control," *Advances in Space Research*, vol. 52, no. 12, pp. 2156–2167, 2013.

[40] R. Wang, S. Tang, and D. Zhang, "Short-range reentry guidance with impact angle and impact velocity constraints for hypersonic gliding reentry vehicle," *IEEE Access*, vol. 7, pp. 47437–47450, 2019.

[41] S. Sun, D. Zhou, and W.-t. Hou, "A guidance law with finite time convergence accounting for autopilot lag," *Aerospace Science and Technology*, vol. 25, no. 1, pp. 132–137, 2013.